Cross section of $^{16}O + ^{16}O$ near the Coulomb barrier

A. Kuronen, J. Keinonen, and P. Tikkanen
University of Helsinki, Accelerator Laboratory, Hämeentie 100, SF-00550 Helsinki, Finland
(Received 14 October 1986)

The partial production cross sections for reaction residues following the $^{16}O+^{16}O$ fusion have been measured at $E_{c.m.}=8.0-13.8$ MeV through γ-ray spectroscopy. The Doppler-shift attenuation method in conjunction with a Ta_2O_5 target and Ge(Li) detector was used to obtain accurate intensities of characteristic γ rays. The results are compared with those of recent experiments.

I. INTRODUCTION

The fusion reaction $^{16}O+^{16}O$ near the Coulomb barrier has been extensively studied in order to understand the effect of the microscopic structure in the fusion of light nuclei[1-8] and the role of the oxygen burning via $^{16}O+^{16}O$ in highly developed massive stars.[5-7] The partial production cross sections for reaction residues have been studied by means of particle[1,2,5] and γ-ray spectroscopy.[3,4,6-8] In spite of the importance of the reaction, the rough agreement between reported studies yields only moderate knowledge on the total cross section. Considering the γ-ray studies, the main reason behind this is that for the partial cross sections the intensities of the characteristic γ rays have been in most cases difficult to obtain due to the overlapping of the strongly Doppler-shifted γ-ray line shapes.

The aim of this work is to complete the most recent study by Thomas *et al.*[8] published during the present experiment. We have used a new approach to obtain the intensities of the characteristic γ rays with a high resolution Ge(Li) detector and Ta_2O_5 as target material: The strongly Doppler-shifted γ-ray peaks were analyzed by the use of the Doppler shift attenuation (DSA) method. In the deduction of the partial cross section values, the published results of the statistical model calculations by Wu and Branes[7] and Thomas *et al.*[8] were utilized.

II. EXPERIMENTAL METHOD AND RESULTS

The 5 MV tandem accelerator EGP-10-II of the laboratory supplied the 20—200 particle nA ^{16}O beams in charge states 4^+ and 5^+ at laboratory energies covering the range from 16 to 28 MeV. The beams were collimated to form a spot of 1×2 mm^2 on the target.

The ^{16}O targets were prepared by anodizing clean 0.4 mm thick Ta metal sheets. The target thicknesses of 290 ± 15 μg/cm^2 (3410 ± 170 Å) and the stoichiometry $Ta_{(1.9\pm0.1)}O_{(5.1\pm0.2)}$ were determined by Rutherford backscattering of 2 MeV α particles from the 2.5 MV van de Graaff accelerator of the laboratory. The target thickness and stoichiometry were determined before and after each series of measurements. Within the experimental uncertainty, no changes were observed. Care was taken to prevent ^{12}C buildup and to ensure accurate relative and absolute normalization of the γ-ray intensities. A liquid-nitrogen-cooled trap was used in the target chamber. The 440 keV (^{23}Na) and 1809 keV (^{26}Mg) peaks arising from the $^{16}O+^{12}C$ reactions were monitored and used to determine the amount of ^{12}C on the target. This enabled a correction to be made for peaks that arise from both $^{16}O+^{12}C$ (cross section from Ref. 9) and $^{16}O+^{16}O$. The intensity of the 302 keV ^{181}Ta line from the Coulomb excitation was used as the standard to obtain the partial cross sections. The value of $B(E2)=0.53\pm0.04$ e^2b^2 (Ref. 10) and the energy and angular distribution dependence according to Ref. 11 were used. The calculated angular distribution was corrected for the solid angle of the detector.[12]

Gamma-ray spectra were accumulated in the energy region from 7.95 to 13.83 MeV c.m. For each value of the cross section the energy loss in the target [from 1.03 MeV at $E_{lab}(^{16}O)=16$ MeV to 0.93 MeV at $E_{lab}(^{16}O)=28$ MeV] was taken into account. The energy loss was calculated by using the scaled stopping power[13] based on the tabulated stopping power data.[14] This procedure is supported by the present DSA analysis. The cross sections were estimated in the middle of the target by using the measured energy dependence. The energy calibration of the beam analyzing magnet was based on the resonances at $E_{lab}(^{15}N)=6385\pm14$ and $17\,350\pm7$ keV in the reaction $^1H(^{15}N,\alpha\gamma)^{12}C$ (Ref. 15) and the very thin H contamination on the surface of each target. The reason behind the use of these resonances is that due to the similar masses of the projectiles, the field strengths for the $^{15}N^{2+,3+}$ and $^{16}O^{4+,5+}$ beams overlap.

The γ radiation was detected in a 120 cm^3 PGT or 80 cm^3 Canberra Ge(Li) detector with the efficiencies of 28% and 18%, respectively. The detectors were located at 0° relative to the beam and 3 cm from the target. Measurements were performed also at angles of 55° and 90° to control the angular distribution dependences of γ-ray yields. The 5 mm Pb, 2 mm Cd, 3 mm Cu, and 2 mm Al sheets were inserted between the target chamber made of stainless steel and a detector to attenuate low-energy x rays and γ rays. The energy resolutions of the detection systems were 2.0 keV (PGT) and 1.9 keV (Canberra) at $E_\gamma=1.33$ MeV and 3.1 keV (PGT) and 2.8 keV (Canberra) at $E_\gamma=2.6$ MeV. The energy and efficiency calibration of the γ detectors was done with ^{56}Co, ^{133}Ba, and ^{152}Eu (Ref. 16) sources placed in the target position.

The data were acquired in steps of about $E_{lab}(^{16}O) = 250$ keV with both increasing and decreasing bombarding energies to further check for carbon buildup on the target and to avoid systematic errors. Four different measurements were performed. Beam-off spectra were measured occasionally to ensure that no correction was needed for residual activity or for laboratory background γ rays.

A typical γ-ray spectrum is shown in Fig. 1. The figure also illustrates Doppler-broadened line shapes of peaks used to obtain the partial cross sections. In deducing the intensities of the Doppler broadened line shapes, Monte Carlo simulations were employed.[17] For the calculation of the slowing down of the recoiling nuclei, the scaled stopping power was taken.[13] The fitting of the calculated and experimental line shapes of the 1369 keV (^{24}Mg) and 1779 keV (^{28}Si) lines confirmed the validity of this approximation. Due to the high recoil velocities [from $\beta = 2.3\%$ for $E_{lab}(^{16}O) = 16$ MeV to 3.1% for $E_{lab}(^{16}O) = 28$ MeV] and thin Ta_2O_5 target, the slowing down dominantly takes place in the Ta backing. The slowing down in Ta_2O_5 was, however, taken into account in the analysis.

The angular distributions of the γ rays used to obtain the partial cross sections were assumed to be isotropic. This assumption was based on the present control measurements at 55° and 90° at several energies, the measurements reported in Ref. 6 and the assumptions justified in Refs. 4 and 7.

The characteristic γ-ray transitions represent only lower limits for the production of the residual nuclei, and the yields have to be corrected for the population of the ground state and the populations of higher lying levels which decay without populating the state whose decay is studied. At low counting rates used, the summing corrections could be neglected. The probabilities that the production of a particular residual nucleus results in a specific γ ray, i.e., the branching factors, are based on the statistical model calculations by Wu and Barnes[7] and Thomas *et al.*[8] For comparison the branching factors were

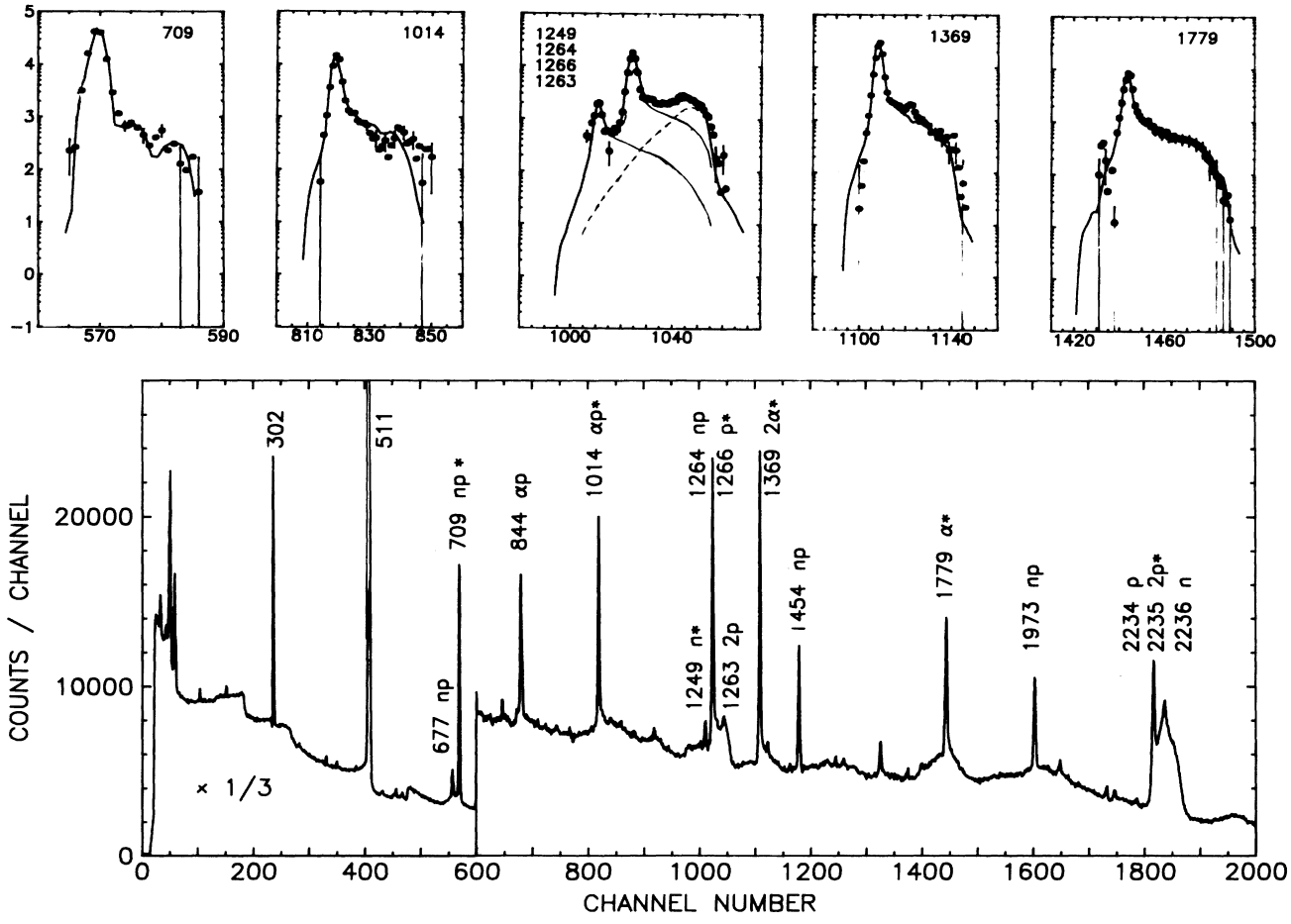

FIG. 1. Typical γ-ray spectrum obtained in the cross section measurements for $^{16}O + ^{16}O$. The conversion gain is 1.2 keV/channel. The spectrum is observed at 27 MeV bombarding energy. The γ-ray peaks are identified by their energy, and the peaks used to deduce the partial cross sections are marked by an asterisk. The upper part shows the portions of the spectrum at these peaks and the Monte Carlo simulations of the line shapes. For clarity, the calculated line shape is not shown for the 1264 keV peak. The dashed line is the simulation of the Doppler broadened 1263 keV line.

TABLE I. Partial and total fusion cross sections (mb) for the $^{16}O+^{16}O$ reaction. The values without the missing yield corrections are given in parentheses.

$E_{c.m.}$ (MeV)	$^{31}S + n$ (1249 keV)		$^{31}P + p$ (1266 keV)		$^{30}Si + 2p$ (2235 keV)		$^{30}P + np$ (709 keV)		$^{28}Si + \alpha$ (1779 keV)		$^{27}Al + \alpha p$ (1014 keV)		$^{24}Mg + 2\alpha$ (1369 keV)		Total cross section	S factor (MeV b)
7.95	(0.0298)	0.069	(0.0546)	0.121	(0.0950)	0.211	(0.0169)	0.113	(0.0684)	0.0919					0.608	1.86×10^{25}
8.25	(0.0362)	0.0844	(0.0861)	0.191	(0.332)	0.706	(0.0412)	0.128	(0.174)	0.235					1.35	1.33
8.45	(0.0688)	0.160	(0.230)	0.511	(0.421)	0.857	(0.0370)	0.218	(0.332)	0.448					2.19	1.06
8.66	(0.0950)	0.222	(0.233)	0.519	(0.879)	1.72	(0.0830)	0.462	(0.533)	0.719					3.65	8.48×10^{24}
8.86	(0.161)	0.373	(0.371)	0.826	(1.61)	3.10	(0.168)	0.884	(0.963)	1.30					6.48	7.73
9.13	(0.278)	0.644	(0.551)	1.23	(2.91)	5.28	(0.333)	1.67	(1.41)	1.91					10.3	5.19
9.34	(0.397)	0.924	(0.844)	1.87	(4.15)	7.28	(0.502)	2.39	(2.26)	3.05	(0.226)	1.27	(0.502)	2.41	19.2	5.06
9.56	(0.555)	1.29	(1.05)	2.34	(5.86)	10.1	(0.884)	4.19	(3.08)	4.16	(0.313)	1.78	(0.715)	3.97	27.8	3.81
9.78	(0.799)	1.86	(1.63)	3.63	(8.70)	14.5	(1.35)	6.08	(4.28)	5.77	(0.564)	3.34	(1.31)	5.68	40.8	2.97
10.00	(1.22)	2.84	(2.44)	5.42	(12.5)	20.2	(1.99)	8.66	(5.46)	7.37	(0.746)	4.23	(1.41)	5.24	53.7	2.12
10.22	(1.45)	3.37	(3.12)	6.93	(16.4)	26.0	(2.66)	11.1	(6.97)	9.46	(1.09)	6.22	(3.03)	9.46	72.4	1.58
10.45	(1.64)	3.81	(4.53)	10.1	(21.4)	33.0	(3.66)	15.2	(9.19)	12.4	(1.88)	10.7	(4.57)	12.7	98.1	1.18
10.67	(1.86)	4.34	(5.51)	12.3	(25.1)	38.1	(4.75)	18.9	(11.4)	15.4	(2.04)	11.6	(4.08)	9.95	111	7.64×10^{23}
10.91	(2.55)	5.95	(6.22)	13.8	(35.5)	52.4	(6.39)	24.6	(13.9)	18.7	(2.87)	16.3	(5.77)	12.9	145	5.55
11.14	(2.81)	6.57	(7.41)	16.5	(47.1)	68.4	(9.01)	34.7	(16.9)	22.9	(4.75)	26.0	(7.99)	16.0	191	4.28
11.37	(2.90)	6.75	(11.1)	24.6	(52.4)	73.7	(10.5)	40.5	(18.8)	25.4	(5.51)	31.3	(11.7)	22.1	224	2.97
11.61	(3.48)	8.08	(11.8)	26.2	(62.2)	86.1	(12.7)	47.1	(20.5)	27.6	(6.79)	11.9	(15.0)	26.9	261	2.03
11.79	(3.65)	8.48	(11.6)	25.8	(69.7)	95.0	(14.0)	51.9	(23.4)	31.6	(8.61)	48.8	(17.2)	26.9	291	1.54
12.10	(3.52)	8.17	(13.5)	29.9	(68.4)	92.8	(15.8)	58.6	(25.2)	34.1	(11.1)	63.0	(29.0)	46.6	333	9.24×10^{22}
12.33	(3.58)	8.30	(14.1)	31.3	(74.1)	99.0	(17.6)	65.3	(25.2)	36.2	(12.1)	68.8	(31.4)	48.4	357	6.22
12.63	(3.02)	7.02	(16.1)	35.8	(81.7)	107	(20.5)	75.9	(27.5)	37.2	(13.2)	75.0	(41.2)	60.8	399	3.87
12.87	(3.25)	7.55	(17.1)	38.0	(91.9)	121	(24.7)	82.1	(29.4)	39.6	(15.1)	86.1	(47.1)	67.0	441	2.72
13.10	(3.30)	7.64	(16.5)	36.7	(105)	136	(25.3)	93.7	(31.6)	42.8	(16.7)	95.5	(54.6)	75.9	488	1.97
13.34	(3.41)	7.95	(16.8)	37.3	(101)	131	(24.7)	91.5	(31.6)	42.8	(17.0)	97.2	(62.2)	83.9	493	1.30
13.58	(2.71)	6.30	(22.6)	50.2	(107)	138	(27.8)	104	(34.5)	46.6	(19.1)	109	(69.7)	92.8	546	9.46×10^{21}
13.83	(2.49)	5.77	(20.4)	45.3	(113)	145	(27.8)	104	(38.1)	51.5	(22.6)	129	(74.1)	98.1	577	6.57

calculated by using the known branching ratios[18] and the $(2J+1)$ rule for the population of the excited states in each residual nucleus. The factors thus obtained are called the missing yield factors in the following.

The characteristic γ-ray transitions used to obtain the partial cross sections given in Table I are discussed in detail in the following:

(a) $n+{}^{31}S$ from 1249 keV. The partial cross section for producing ^{31}S was obtained from the transition 1.25→0 MeV. The mean lifetime $\tau(E_x=1.25\ \text{MeV})=720\pm180$ fs (Ref. 18) leads to that only 52% of the total peak intensity is in the stop peak. The Doppler-shifted part of the peak is below the 1263 keV (^{30}Si), 1264 keV (^{31}P), and 1266 keV (^{31}P) peaks.

The branching factor 0.47 is reported[7,8] to be almost constant over the energy region from 8 to 14 MeV c.m. The missing yield factor 0.43 was used in the present work.

(b) $p+{}^{31}P$ from 1266 keV. The partial cross section for producing ^{31}P was obtained from the transition 1.266→0 MeV. The mean lifetime $\tau(1.266)=750\pm50$ fs (Ref. 18) leads to that about 43% of the total γ-ray intensity was Doppler shifted from the stop peak. The contamination due to the 1263 keV transition 3.50→2.24 MeV in ^{30}Si was shifted above the 1266 keV peak [$\tau(3.50)=83\pm7$ fs (Ref. 18)] and could well be resolved by the use of the DSA analysis. The contamination due to the 1264 keV transition 1.97→0.71 keV (the 59% branch) in ^{30}P was taken into account in the analysis by the use of the 41% branching γ ray at 1973 keV (Ref. 18). The intensity of the contamination was from 5% ($E_{\text{c.m.}}=8$ MeV) to 46% (14 MeV) compared with that of the 1266 keV peak. Due to the long lifetime $\tau(1.97)=4.9\pm1.8$ ps (Ref. 18), 91% of the total intensity is in the stop peak.

The statistical model calculations[7,8] show that the branching factor 0.47 is constant for the 1266 keV transition. The missing yield factor 0.45 was used in the present work.

(c) $2p+{}^{30}Si$ from 2235 keV. The partial cross section for producing ^{30}Si was obtained from the transition 2.24→0 MeV. Due to the lifetime $\tau(2.24)=360\pm20$ fs (Ref. 18) 67% of the intensity of this transition is in the broad flight peak at 2245 keV. The contaminations due to the transition 2.236→0 MeV [$\tau(2.236)=320\pm80$ fs (Ref. 18)] in ^{31}Si and 2.234→0 MeV [$\tau(2.234)=361\pm13$ fs (Ref. 18)] in ^{31}P could be resolved only by using the intensities of the transitions 1.249→0 MeV in ^{31}Si and 1.266→0 MeV in ^{31}P. The intensities were corrected with the ratio of the missing yield factor 0.213 ($E_\gamma=2236$ keV) to 0.43 (1249) in the n channel and 0.312 (2234) to 0.45 (1266) in the p channel. In these one-particle channels the branching factors are constant. The intensity in the n channel varied (with the increasing bombarding energy) from 10% to 1%, and in the p channel from 25% to 11% of the total intensity.

In the two-particle emission, the kinetic energies of the protons are so low that the transmission coefficients strongly affect the branching factor. The missing yield factor of the 2235 keV peak ranged from 0.40 to 0.80. The value 0.80 is observed also from the statistical model calculations.[7,8]

(d) $np+{}^{30}P$ from 709 keV. The partial cross section for producing ^{30}P was obtained from the transition 0.71→0 MeV. Due to the long lifetime $\tau(0.71)=49.7\pm1.1$ ps (Ref. 18), 94% of the total intensity of the transition is in the stop peak.

The missing yield factor in this two-particle channel ranged from 0.12 to 0.30. The value 0.30 corresponds to the results of the statistical model calculations.[7,8]

(e) $\alpha+{}^{28}Si$ from 1779 keV. The partial cross section for producing ^{28}Si was obtained from the transition 1.78→0 MeV. Due to the lifetime $\tau(1.78)=700\pm20$ fs (Ref. 18), the stop peak contains 63% of the total γ intensity.

In this one-particle channel the branching factor is almost constant (about 0.80).[7,8] The missing yield factor of 0.74 was used in the present work.

(f) $\alpha p+{}^{27}Al$ from 1014 keV. The partial cross section for producing ^{27}Al was obtained from the transition 1.014→0 MeV. Due to the lifetime $\tau(1.014)=2.12\pm0.08$ ps (Ref. 18), the stop peak contains 78% of the total intensity. The γ-ray yields were corrected for the ^{16}O+^{12}C reaction contamination. Because of the uncertainties due to the carbon contamination, the small cross section values below $E_{\text{c.m.}}=9.34$ MeV are not reported.

The missing yield factors in this two-particle channel ranged from 0.02 to 0.09. The factor 0.09 corresponds to the results of the statistical model calculations.[7,8]

(g) $2\alpha+{}^{24}Mg$ from 1369 keV. The partial cross section for producing ^{24}Mg was obtained from the transition 1.37→0 MeV. Due to the lifetime $\tau(1.37)=1.98\pm0.04$ ps (Ref. 18), the stop peak represents 79% of the total γ intensity. The intensities obtained were corrected for the ^{16}O+^{12}C reaction contamination. Very small cross section values observed below $E_{\text{c.m.}}=9.34$ MeV are not reported.

The branching factor used ranged from 0.03 to 0.75. The saturation value of the statistical model calculations[7,8] corresponds to the missing yield factor 0.85.

The uncertainty of the reported partial cross section is 15% in the n channel, 21% in the p channel, 19% in the 2p channel, 10% in the np channel, 17% in the α channel, 20% in the αp channel, and 20% in the 2α channel. It includes the uncertainties in the target thickness and stoichiometry (5%), measured γ-ray yield of the Coulomb excitation (less than 1%), missing yield factor (10% for the α, p, 2p, and n channels; 15% for the 2α, np, and αp channels), photopeak efficiency (2%), and statistical uncertainties in the γ-ray yields with the inclusion of the uncertainties due to the contaminations. The uncertainty in the total cross section values is 20% resulting from the uncertainties of the partial cross sections and the uncertainty of the $B(E2)$ standard.

III. COMPARISON WITH PREVIOUS RESULTS

The present partial cross sections are compared in Fig. 2 with the results of the recent measurements by Hulke *et al.*,[6] Wu and Barnes,[7] and Thomas *et al.*[8] All the channels studied in the present work have been previously resolved only in Refs. 7 and 8.

The disagreements between the present and previous results can mostly be explained by the unresolved Doppler-

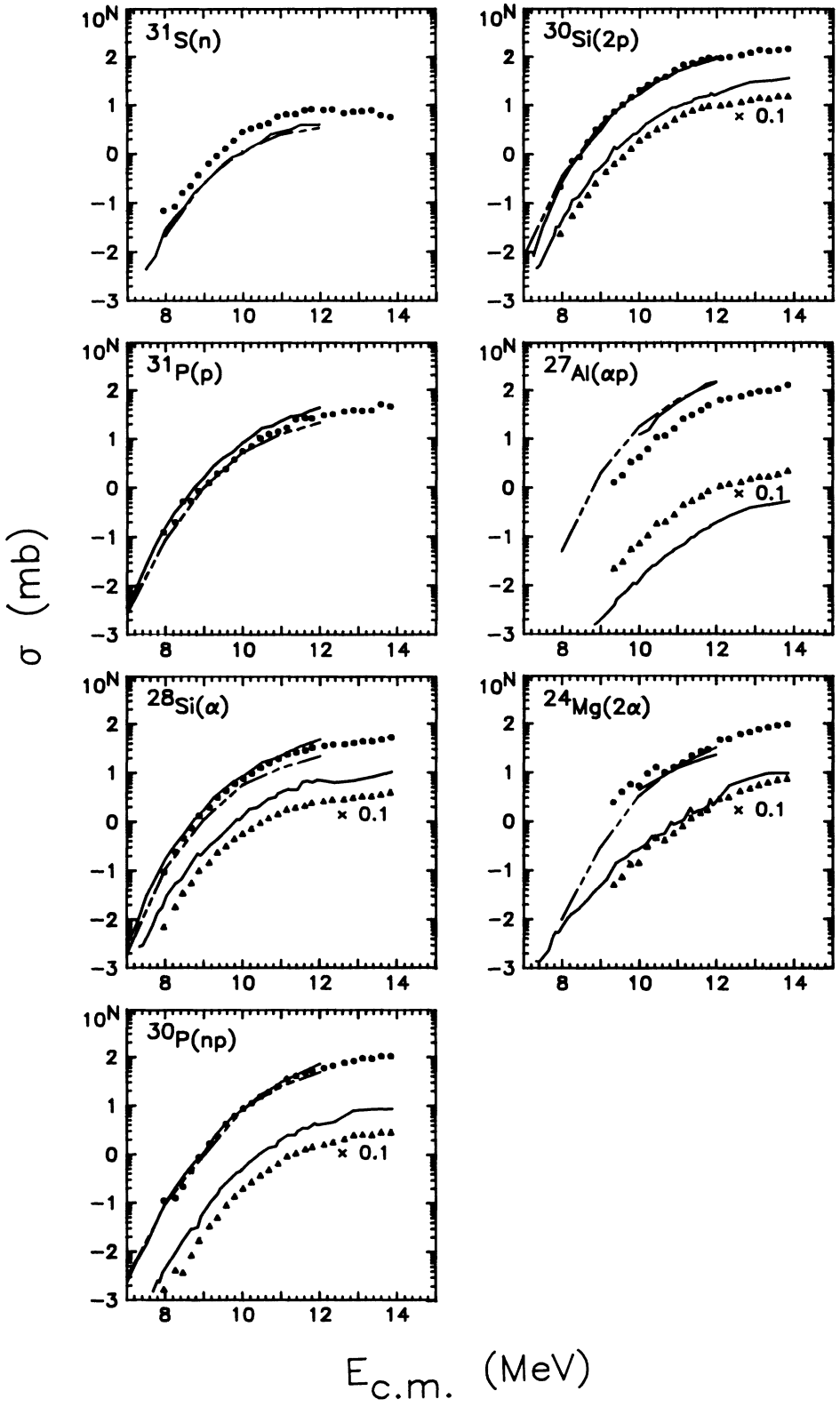

FIG. 2. Partial fusion reaction cross sections (circles) in the $^{16}O + ^{16}O$ fusion compared with the values by Wu and Barnes (Ref. 7) (solid line) and Thomas *et al.* (Ref. 8) (dashed line). The present γ-ray yields (triangles) are also compared with the results by Hulke *et al.* (Ref. 6) (solid line).

broadened line shapes and the difficulties in evaluating the background under these γ peaks. Note that due to the line shape fitting, the peak intensities deduced in the present work are not sensitive to the background around the γ peak.

In the case of the n channel (^{31}S), the present cross sections are by about a factor of 2 higher than those of Ref. 8. This channel was not resolved in Ref. 6. By considering the deconvolution shown in Fig. 1 and the fact that only about 52% of the γ-ray yield can be observed in the stop peak, this disagreement can be explained. The use of a SiO_2 target in Ref. 7 leads to even higher loss of intensity from the stop peak than in the case of a Ta_2O_5 target (the present work and Ref. 8).

Within the given uncertainties the present p channel (^{31}P) cross sections are in agreement with those of Refs. 7 and 8. The reason behind the fact that the values in Ref. 7 are systematically higher could be the n-channel contamination in these measurements with the slow stopping material SiO_2.

In the case of the α channel (^{28}Si), the present 1779 keV γ-ray yields are by about a factor of 2 lower than those of Ref. 6. Within the given uncertainties the present cross section values are in agreement with those of Refs. 7 and 8. The systematic deviation from the results of Ref. 8 could be due to the difficulties in evaluating the background.

The present cross sections of the np channel (^{30}P) (and the d channel at higher energies) are in agreement with those reported in Refs. 7 and 8, whereas the yields of the 709 keV γ rays are by about a factor of 2 lower than those reported in Ref. 6.

In the case of the 2p channel (^{30}Si) the strongest characteristic γ-ray peak is contaminated by the γ rays from the p and n channels. Due to the practically same lifetimes, the resolution of different channels was done by using the relative intensities of the transitions 1.249→0 MeV (^{31}Si) and 1.266→0 MeV (^{31}P). Thus, the γ yield deduced to the 2p channel depends on the accurate deconvolution of the 1.27 MeV group. the present cross section values are in agreement with those reported in Refs. 7 and 8. By comparing the total γ intensities of the 1.26 and 2.24 MeV groups with those given in Ref. 6, disagreement can be observed.

TABLE II. Comparison of the total cross section for the $^{16}O+^{16}O$ reaction at 12 MeV.

σ_{fus} (mb)	Detection	Ref.
420±100	light particles	5
220±20	heavy residues	1
150±10		2
330±20[a]	γ rays	4
480±40[a]		3
540±120[a]		6
440±70[a]		7
400±30		8
320±70		this work

[a]The missing yield corrections are according to Ref. 7.

The cross sections obtained for the αp channel (^{27}Al) are, by about a factor of 2, lower than the values given in Refs. 7 and 8. The comparison of the 1014 keV γ-ray yields with those given in Ref. 6 shows that the present yields are higher by about a factor of 5. These discrepancies cannot (at higher energies) be explained as being due to the carbon contamination in the present work; the correction in the γ-ray yield was about 7% in the worst case.

The γ yields characterizing the 2α channel (^{24}Mg) are, within the given uncertainties, in agreement with those reported in Ref. 6, as are the partial cross sections with those reported in Refs. 7 and 8.

The present total cross sections given in Table I are compared with the previous results in Table II. The main reason behind the disagreement between the present total cross section and that by Thomas *et al.*[8] is due to the αp channel.

In conclusion, the measurements and analysis of γ-ray yields for the partial cross sections of the $^{16}O+^{16}O$ fusion reaction at sub-barrier energies are described in detail. The emphasis has been put on resolving different channels by the use of the DSA method in the deduction of the γ-ray yields.

This work has been partially financed by the Academy of Finland.

[1]I. Tserruya *et al.*, Phys. Rev. C **18**, 1688 (1978).
[2]D. G. Kovar *et al.*, Phys. Rev. C **20**, 1305 (1979).
[3]J. J. Kolata *et al.*, Phys. Rev. C **19**, 2237 (1979).
[4]V. K. C. Cheng *et al.*, Nucl. Phys. **A322**, 168 (1979).
[5]H. Spinka and H. Winkler, Nucl. Phys. **A233**, 456 (1974).
[6]G. Hulke, C. Rolfs, and H. P. Trautvetter, Z. Phys. A **297**, 161 (1980).
[7]S.-C. Wu and C. A. Barnes, Nucl. Phys. **A422**, 373 (1984).
[8]J. Thomas *et al.*, Phys. Rev. C **33**, 1679 (1986).
[9]P. R. Christensen, Z. E. Switkowski, and R. A. Dayras, Nucl. Phys. **A280**, 189 (1977).
[10]R. B. Firestone, Nucl. Data Sheets **43**, 289 (1984).
[11]K. Alder and A. Winther, *Coulomb Excitation* (Academic, New York, 1966).
[12]D. C. Camp and A. L. van Lehn, Nucl. Instrum. Methods **76**, 192 (1969).
[13]J. F. Ziegler, Appl. Phys. Lett. **31**, 544 (1977).
[14]H. H. Andersen and J. F. Ziegler, *The Stopping and Ranges of Ion in Matter*, Vol. 3 of *Hydrogen Stopping Powers and Ranges in All Elements*, edited by J. F. Ziegler (Pergamon, New York, 1977).
[15]B. Maurel and G. Amsel, Nucl. Instrum. Methods **218**, 159 (1983); F. Ajzenberg-Selove, Nucl. Phys. **A375**, 1 (1982).
[16]*Table of Isotopes*, 7th ed., edited by C. M. Lederer and V. S. Shirley (Wiley, New York, 1978).
[17]J. Keinonen, in *Capture Gamma-ray Spectroscopy and Related Topics—1984*, Proceedings of the International Symposium on Capture Gamma-ray Spectroscopy and Related Topics, AIP Conf. Proc. No. 125, edited by S. Raman (AIP, New York, 1985), p. 557; P. Tikkanen *et al.*, Nucl. Phys. **A456**, 337 (1986).
[18]P. M. Endt and C. van der Leun, Nucl. Phys. **A310**, 1 (1978).